

Photonic Integrated Circuits based on Sampled-Grating Distributed-Bragg-Reflector Lasers

Jonathon S. Barton, Erik J. Skogen, Milan Mašanovic, James Raring, Matt Sysak, Leif Johansson, Steven P. DenBaars, Larry A. Coldren

University of California, Santa Barbara, Santa Barbara CA 93106

ABSTRACT

The Sampled-Grating Distributed-Bragg-Reflector laser (SGDBR) provides wide tunability ($>40\text{nm}$), and high output power ($>10\text{mW}$). Driven by the demand for network re-configurability and ease of implementation, the SGDBR has moved from the research lab to be commercially viable in the marketplace. The SGDBR is most often implemented using an offset-quantum well epitaxial structure in which the quantum wells are etched off in the passive sections. Alternatively, quantum well intermixing has been used recently to achieve the same goal - resulting in improved optical gain and the potential for multiple band-gaps along the device structure. These epitaxial 'platforms' provide the basis for more exotic opto-electronic device functionality exhibiting low chirp for digital applications and enhanced linearity for analog applications. This talk will cover state-of-the-art opto-electronic devices based on the SGDBR platform including: integrated Mach-Zehnder modulators, and integrated Electro-absorption modulators.

Keywords: Tunable lasers, Modulators, Optoelectronics, SGDBR, Chirp, Linearity

1. Introduction

Tunable lasers are desirable for a number of applications such as in networks requiring dynamic provisioning, the replacement of Distributed Feedback (DFB) lasers in Wavelength Division Multiplexing (WDM) systems, in phased radar systems, or for optical switching, and routing[1]. Recently, single-wavelength DFBs have been integrated with Electro-absorption modulators (EAMs)[2] and Mach-Zehnder (MZ) interferometric-based modulators[3]. Widely-tunable Sampled-Grating DBR lasers(SGDBR) have also been integrated with various components over the last few years such as Semiconductor Optical Amplifiers (SOAs)[4], EAMs [5], Mach-Zehnder modulators [6,7], and wavelength monitors. Integration leads to reduced costs in packaging, lower insertion losses, and advanced functionality in more complex photonic integrated circuits (PICs), despite potential problems of optical and electrical crosstalk. In this paper, we will examine a few of the latest integrated photonic devices based on the SGDBR platform as described below.

First we will look at integrated SGDBR- MZ devices. This type of modulator is preferable due to its superior power handling with less photocurrent generation than EAM devices and ease in generation of tailorable chirp. These MZ modulators also can provide low drive voltage – a trade-off with insertion losses in the device. Secondly, an integrated SGDBR – EAM device is examined that incorporates quantum-well intermixing technology with a buried ridge stripe fabrication approach. This approach excels due to the ability to fashion multiple band-gaps across the device – leading to optimization of each section – passive, modulator, and active.

1.1. SGDBR Platform

The SGDBR itself consists of four sections; gain, phase, front mirror, and back mirror. The front and rear mirrors consist of periodically sampled DBR gratings to form a comb-like reflectivity spectrum[9]. The sampling periods in the front and back mirrors differ, which provides a different peak reflectivity spacing, so that only one set of mirror reflectivity peaks is aligned within the desired tuning range. By differentially tuning the front and back mirrors a small amount, adjacent reflectivity peaks can be aligned, and the laser will operate at this new wavelength [9]. Due to the fact that the mirrors are lithographically defined and require no facet reflections, integration with other components becomes fairly simple. Due to the compatibility of the different fabrication steps in the SGDBR, SOA, detector, Mach-Zehnder, and EAM sections, fabrication of an integrated device is no more difficult than fabrication of a SGDBR itself. Of the three different designs presented in this work, the MZ-SGDBR uses a ridge based SGDBR design. The SGDBRs use a 5 period front sampled-grating mirror with $4\mu\text{m}$ bursts and a 12 period rear sampled-grating mirror with $6\mu\text{m}$ bursts. The tunable laser length is 1.55mm, consisting of the gain section ($550\mu\text{m}$), phase section ($75\mu\text{m}$), front and rear mirrors, and rear absorber section ($100\mu\text{m}$).

A backside absorber has been monolithically integrated to reduce reflection from the back facet. Reflections back into the laser are detrimental and require minimization. This can be accomplished by using a few approaches. The MMI lengths are optimized for minimum reflections and are tapered so that reflections are not coupled back into the laser cavity – mostly important in the ‘off’ state. Additionally, the waveguide design is weakly guided and a multi-layer AR coating is employed. The waveguide is continuous throughout the structure – including active and passive sections avoiding any potential index discontinuities such as might be found at butt-coupled regrowth interfaces. The last EAM-SGDBR uses a buried hetero-structure design outlined in its respective section.

2. MZ-SGDBR Devices

2.1. Introduction

In high bit-rate digital modulation systems ($\geq 10\text{Gbit/s}$), the combination of excess laser bandwidth due to chirp and fiber dispersion can limit the link’s reach. Because of this, tailorable chirp modulators are preferable to generate both high-speed modulation and either negative or zero chirp depending on the application. Historically discrete LiNbO_3 Mach-Zehnder modulators have been used to achieve high performance. The aim of this device is to fabricate a compact transmitter that can simultaneously provide wide tunability, tailorable chirp, low insertion loss, low drive voltage requirements, and high speed.

2.2. Device Layout

First generation devices consisted of the integration of a ridge-based SGDBR as described in Section 1.1 with a MZ section having $550\mu\text{m}$ long electrodes as shown in Fig. 1. First generation Mach-Zehnder devices utilized two multimode interference (MMI) combiners/splitters ($97\mu\text{m}$ long, $9.5\mu\text{m}$ wide) with curved waveguides extending to a separation of $40\mu\text{m}$ in between the two branches. This yields a modulator length of 1.2mm with a total device length of 2.75 mm. In order to decrease the insertion losses, 2nd Generation devices included a $400\mu\text{m}$ integrated SOA before the MZ section. Also, a forward biased phase shifter was added in order to better control the device phase branch differential over the wavelength range to yield optimum extinction and to overcome fabrication inconsistencies. 2nd Generation device branch waveguides were separated by $20\mu\text{m}$ with a $97\mu\text{m}$ long, $9.5\mu\text{m}$ wide 1x2 MMI and a $170\mu\text{m}$ long, $10.5\mu\text{m}$ wide 2x2 MMI with MZ pad electrodes consisting of $200\mu\text{m}$, $250\mu\text{m}$ and $300\mu\text{m}$ as shown in Fig. 2. This yields a modulator length of 1.1mm for the 2nd Generation devices including a $250\mu\text{m}$ curved waveguide output. The total device length is 3.3mm long.

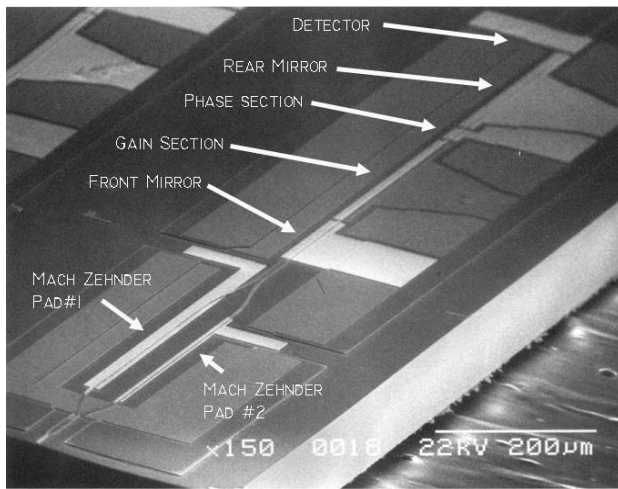


Figure 1 1st Generation MZ-SGDBR electron micrograph

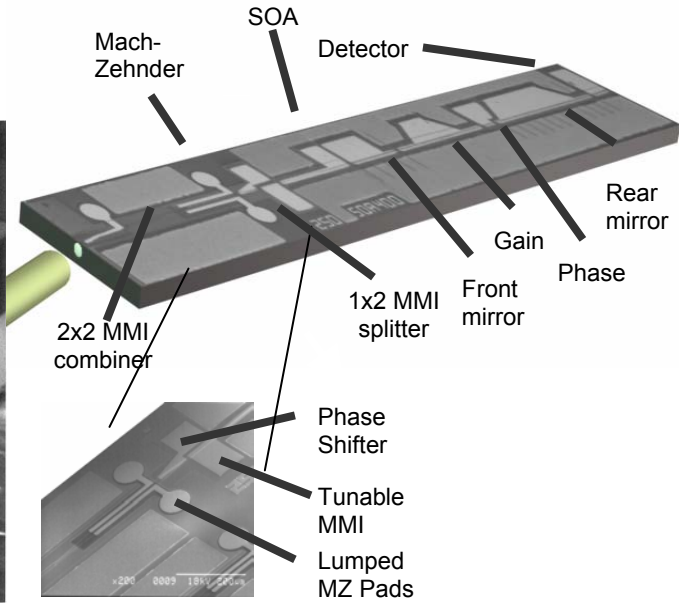


Figure 2 2nd Generation MZ-SOA-SGDBR Device layout

These designs use a common quaternary waveguide structure in which the modulator and passive sections are formed by etching off the QWs down to the 10nm InP stop-etch layer as shown in Fig. 3. The active epi-layer structure consists of an offset quantum well structure (QW) as shown in Table 1. These devices use the same doping/composition structure in the modulator, mirrors and phase sections for ease of fabrication. Thus, tradeoffs in design must be considered. In order to achieve adequate wavelength tuning (40nm) the band-edge (1.4Q) needs to be fairly close to the operating wavelength without increasing the on-state internal loss excessively. The modulator section becomes increasingly efficient as the composition approaches the band-edge as well due to higher order electro-optic effects. Ideally, the band-gap of different sections can be tailored by using quantum well intermixing. This approach will be explored in Section 4.

TABLE I EPI-LAYER STRUCTURE

Layer	Thickness (nm)	Composition – Doping
InGaAs	100	$1 \times 10^{19} \text{ cm}^{-3} \text{ Zn}$
<i>p</i> -InP	1800	$1 \times 10^{18} \text{ cm}^{-3} \text{ Zn}$
1.226LM 7QWs	25	nid 8nm barriers 6.5nm wells
InP stopetch	10	nid
Waveguide	350	1.4Q $1 \times 10^{17} \text{ cm}^{-3} \text{ Si}$
n-InP	1800	$1 \times 10^{18} \text{ cm}^{-3} \text{ Si}$
Buffer		
S Doped Substrate	100000	$5 \times 10^{18} \text{ cm}^{-3} \text{ S}$

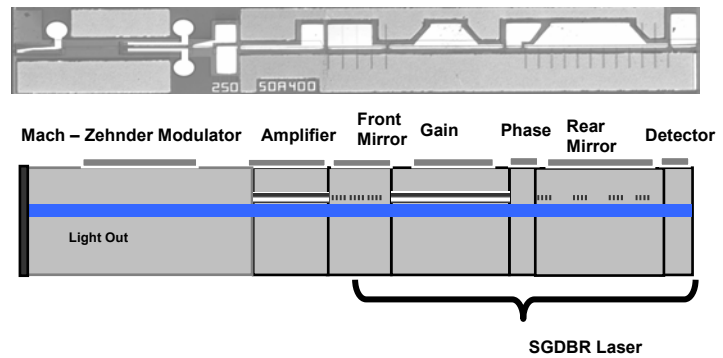


Figure 3. Integrated Device Side View

2.3. RESULTS

DC extinction data is shown for a 550 μm length electrode MZ in Fig. 4. DC extinction characteristics are similar over the wavelength range with greater than 18dB. In order to maximize the extinction ratio the DC bias needs to be optimized for each wavelength. Also, small-signal chirp measurements are shown in Fig. 4 with a one-sided modulation format based on the measurement approach in [10].

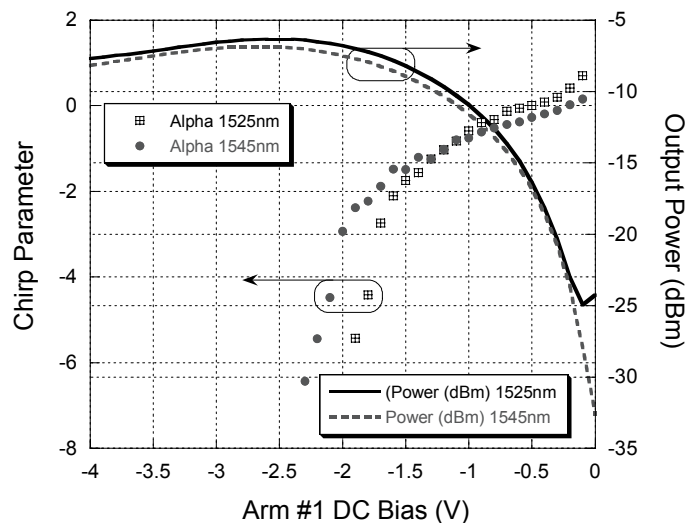


Figure 4 Chirp Parameter as a function of DC extinction curve for pi-shifted case with 550 μm device (1.38 μm waveguide)

As expected, with the device biased with a pi-shift in phase, the chirp parameter is negative in the region when the device is turned 'on' and positive when turned 'off'. By controlling the DC biases, large-signal chirp can be tailored as desired. Improved chirp characteristics can be achieved using a push-pull modulation scheme.

2nd Generation devices make use of integrated SOA before the MZ modulator. This active section provides not only added gain, but helps to even out the wavelength dependent power variation as the gain is higher for lower optical input powers. Figure 5 shows the gain characteristics as a function of current bias on the SOA for different lengths of devices.

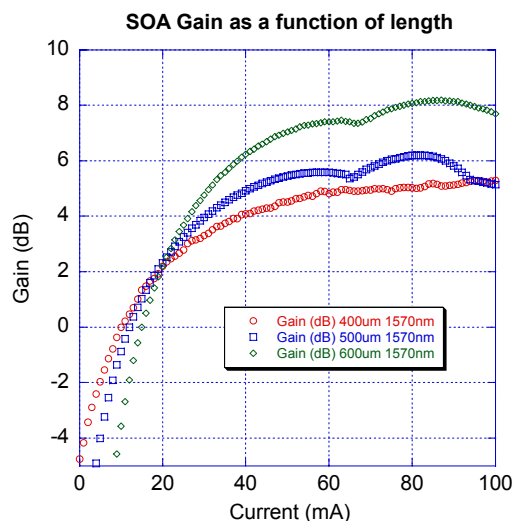


Figure 5 SOA gain with 100mA on Gain section of SGDBR

2.4. Device Bandwidth

Using a low k dielectric such as BCB lowers the parasitic capacitance of the ridge structure considerably. Second Generation devices use a 300nm SiO₂ / 2um BCB / 100nm SiO₂ sandwich of dielectric beneath the electrode pads as shown in Fig. 7. Figure 8 shows a comparison of the electrical/optical S₂₁ for different length MZ pads under one sided modulation. Each is shown for a bias of -4V. For each length as the depletion region is extended with reverse bias, the bandwidth is improved. This corresponds to a 3-4GHz change with bias from -1V to -4V.

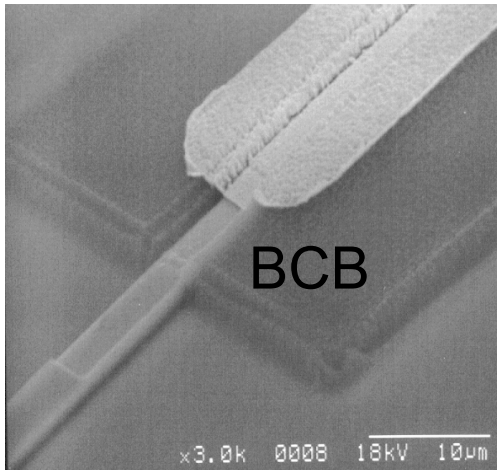


Figure 7 Pad on SiO₂/BCB/SiO₂ low k-dielectric

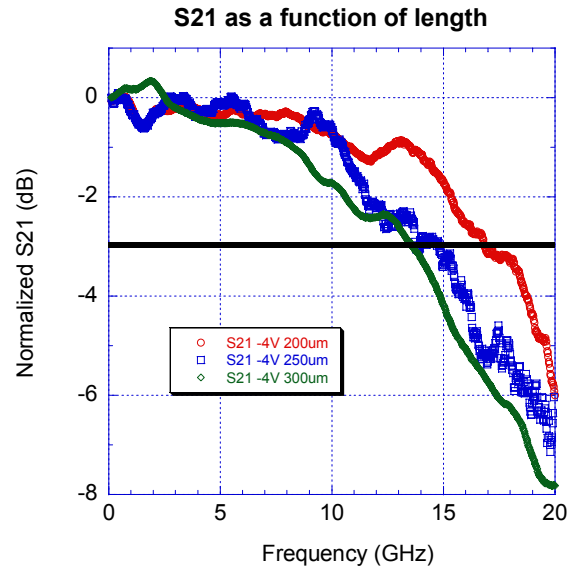


Figure 8 Normalized S₂₁ for different device lengths at -4V Bias

2.5. Conclusion

We have demonstrated monolithic integration of SGDBR-MZ and SGDBR-SOA-MZ devices. These devices have static DC extinction ratios greater than 18 dB. Second Generation devices demonstrate adequate 3dB bandwidth for 10 Gbit/s operation along with the chirp tailorability inherent in the Mach-Zehnder design.

3. Quantum well intermixed integrated SGDBR-EAM

3.1. Introduction

The monolithic integration of several opto-electronic components requires each portion to possess a specific band edge for optimal performance. For example, each section of the sampled-grating DBR laser should be designed with band edges specific to the function of the particular section. Quantum well intermixing allows for the as-grown active region to be shifted precise amounts in the mirror and phase sections to achieve low propagation loss while attaining high tuning efficiency.

This concept can be extended to more complex photonic integrated circuits requiring several band-edge specific components. A good illustration of an integrated circuit requiring a third band-edge is the integration of an EAM with an SGDBR. The band-edge in the EAM should be such that in the unbiased state the propagation loss due to absorption is not significant while under a reasonable reverse bias, the necessary extinction is achieved. Using the same band-edge that has been optimized for the passive components for the EAM requires application of larger than desired voltages necessary to obtain significant signal extinction. Clearly, an EAM band-edge intermediate to the active and passive sections of the SGDBR would be favorable. With QWI technology, this can be achieved on a single chip.

The QWI technology not only allows for the realization of three or more specific band edges, but also permits the use of the centered quantum well design. The optical mode overlap with the centered quantum wells is improved by 50% over the offset quantum well design, thus increasing the modal gain, and reducing the threshold current. Also, because QWI does not change the average composition, and only slightly changes the compositional profile, there is a negligible index discontinuity at the active/passive interface. This eliminates the parasitic reflections that can degrade device performance.

3.2. Quantum Well Intermixing Background

There are several techniques used to accomplish QWI, impurity-induced disordering (IID) [17], the impurity-free vacancy-enhanced disordering (IFVD) [18], [19], and photoabsorption-induced disordering (PAID) [20] are just a few.

In this work we employ the implant enhanced inter-diffusion method, which relies on the diffusion of point defects, specifically vacancies, created during an ion implantation. This method has been shown to have good spatial resolution, and be controllable using anneal time, temperature, and implant dose [20]. Wide ranges of implant energies have been used in this process from the MeV range down to tens of keV. Commonly, these implants are performed on full laser structures, where the vacancies are created in the upper cladding, and must diffuse long distances before reaching the quantum wells. Although this is not detrimental to the intermixing itself, the device performance may be hindered by the redistribution of precisely placed doping interfaces. This can be avoided by using a partially grown laser structure and a sacrificial cap layer which can be subsequently removed and the upper cladding regrown as described in [21]. While this demonstrated such a concept, the process was not optimized, as multiple implant and anneal cycles were required to achieve significant intermixing.

3.3. EAM Design

Electro-absorption modulators have been monolithically integrated with the SGDBR, and were spaced 10 microns ahead of the front SGDBR mirror. The mask was such that single section EAMs of varying lengths were included. A schematic of one of the integrated circuits is shown in Fig. 12. Since QWI only smears the interfaces between the quantum wells and barriers, the quantum wells still remain after the intermixing is completed. This allows for the exploitation of the quantum confined Stark effect in the EAM.

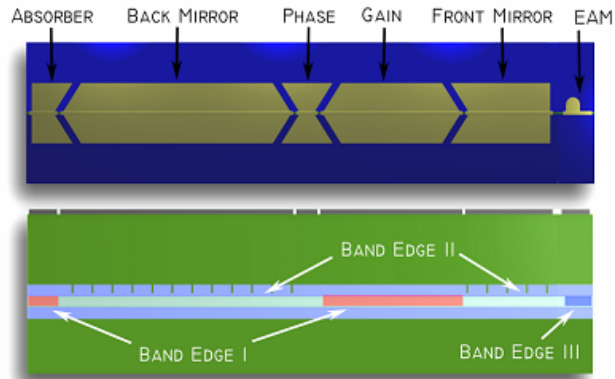


Figure 12. SGDBR-EAM Device Layout

3.4. Process

The epitaxial base structure, shown in Fig. 13, was grown on a sulfur doped InP substrate using a Thomas Swan horizontal-flow rotating-disc MOCVD reactor. The active region consists of either seven or ten 7.0 nm compressively strained (1.3%) quantum wells, separated by 8.0 nm tensile strained (0.3%) barriers, centered within two 1.3Q layers designed to optimize the optical mode overlap with the quantum wells. Following the active region, a 15 nm InP stop etch, a 20 nm 1.3Q stop etch, and a 450 nm InP implant buffer layer was grown.

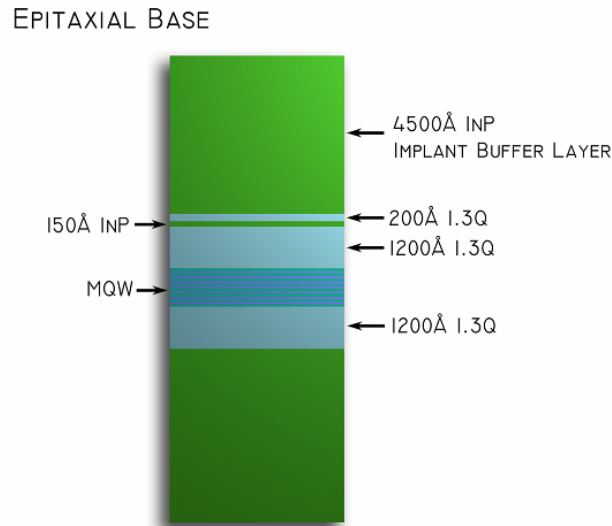


Figure 13. Base growth structure

The active regions were masked with 500 nm of Si_xN_y , and an ion implant was carried out using P^+ at an energy of 100 keV, yielding a range of 90 nm, with a dose of $5 \times 10^{14} \text{ cm}^{-2}$, using a substrate temperature of 200 °C [15]. The implant buffer layer was designed to completely capture the ion implant, creating vacancies far from the active region.

These vacancies were then partially diffused through the structure during a 90-second, 675 °C rapid thermal anneal (RTA), yielding the desired band-edge for the EAM. The implant buffer layer above the EAM sections was removed using a wet etching process, stopping on the 1.3Q stop etch layer. The sample was then subjected to an additional 110-

second rapid thermal anneal blue-shifting the regions where the implant buffer layer remained. This second anneal was used to obtain desired band edge for the mirror and phase sections. The remaining implant buffer layer and 1.3Q stop etch layers were removed using a wet etch process, leaving a thin planar InP surface just above the waveguide. This gives access to the high field region of the optical mode, which is ideal for etching high coupling coefficient gratings, on the order of 300 cm^{-1} , directly into the waveguide.

The sampled grating mirrors were defined by RIE etching deep gratings, 800Å , directly into the waveguide through a Si_xN_y sampling mask. The gratings were then planarized using an optimized MOCVD regrowth. Following the planarizing regrowth, a ridge was RIE etched through the waveguide structure, etch damage was removed using a bromine-based polishing etch. The ridge was buried in p-type InP with an InGaAs contact layer during a second MOCVD regrowth designed to yield a planar buried ridge stripe (BRS) geometry. The contact layer was etched to a width of $6\text{ }\mu\text{m}$, positioned directly above the original etched ridge. A proton implant was performed along side the laser and EAM structures to reduce current leakage and parasitic capacitance in the device [14]. A blanket of Si_xN_y was deposited 200 nm thick, and a via to the contact layer etched to facilitate the Ti/Pt/Au contact, patterned using a liftoff process. The substrate was lapped to a thickness of $90\text{ }\mu\text{m}$, and a Ti/Pt/Au contact was deposited for the back-side n-contact. The devices were cleaved into bars and anti-reflection coated. The die were separated, soldered to aluminum nitride carriers, and wire bonded, for continuous-wave testing.

3.5. Quantum Well Intermixing Results

The intermixing process was calibrated using several samples cleaved from an implanted seven quantum well base structure, as described in the previous section. These samples were annealed at 675°C for various times ranging from 30-seconds to 300-seconds at 30-second intervals and the extent of the intermixing was measured by room-temperature photoluminescence. As the vacancy front moves through the quantum well region the blue-shift increases linearly. Once the vacancy front has moved through the quantum well region there is a saturation of the blue-shift. This saturation of the blue-shift can be observed above 120 nm as shown in Fig. 14.

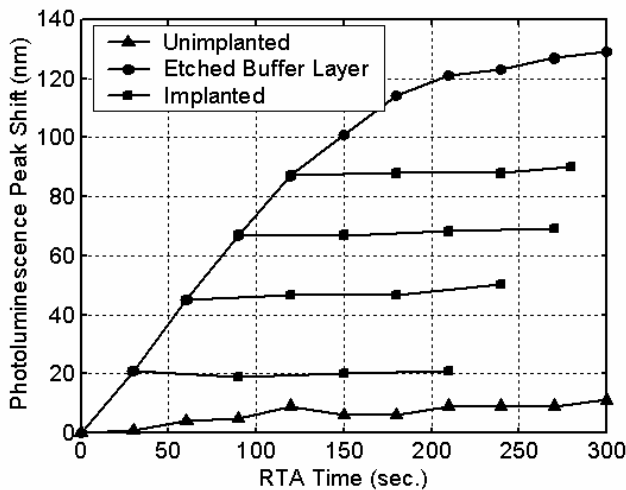


Figure 14. PL Shift as a function of RTA time

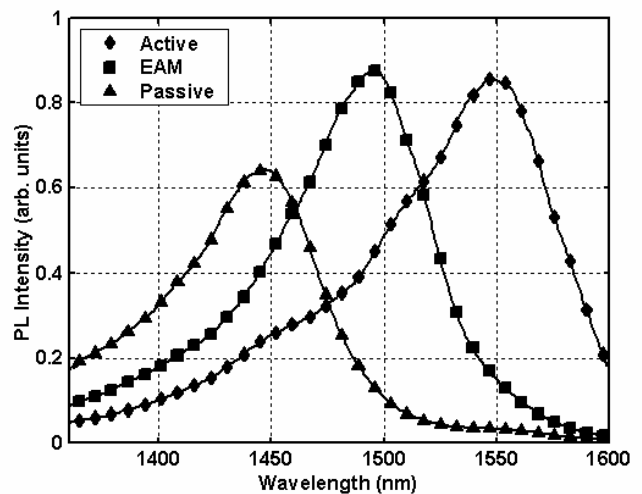


Figure 15. PL intensity for the three different sections

After the 30, 60, 90, 120-second anneals, the implant buffer layer was removed from the respective samples. These samples were then subjected to additional anneal cycles. We found that removing the implant buffer layer halted the blue-shift during these anneals. The arrest of the blue-shift is the result of the removal of the abundance of vacancies, necessary for intermixing, along with the implant buffer layer.

With this process it is possible to achieve any number of band-edges across the wafer, limited only by the practical number of lithographic process steps. For this work, only three band-edges were needed, the as grown bandgap for the

gain regions, a band-edge ideal for the mirror and phase tuning sections, and an intermediate band-edge for the EAM.

We found the quality of the QWI material in all three regions to be quite good as characterized by the peak intensity and FWHM of the photoluminescence curves. The photoluminescence curves for a ten quantum well sample, used in this work, are shown in Fig. 15.

3.6. Active/Passive Fabry-Perot BRS Lasers

An important parameter in the SGDBR device is the modal loss in the mirror and phase sections at the gain peak of the active region. Not only does the modal loss in these regions have a large effect on the un-tuned output power of the device, but also, plays a large role in determining the power ripple in the tuning band. Using active/passive devices, where the passive region is composed of intermixed quantum wells, the modal loss of the intermixed quantum wells, used in the mirror and phase sections, can be extracted. This is done by plotting the differential efficiency of the active/passive device as a function of passive region length. The tuning and EAM region modal loss was computed to be 5.1 cm^{-1} and 8.0 cm^{-1} , respectively.

3.7. Carrier Induced Tuning

In order to cover the full tuning range in our SGDBR design, the front mirror must continuously tune 7 nm by a carrier-induced change in refractive index. A more detailed description of the theory behind SGDBR tuning is given in [9]. The tuning of a 7 quantum well sample was measured by examining the below threshold spectra as a function of bias. The results of this measurement are shown in Fig. 16, where we have demonstrated over 7 nm of continuous tuning, which translates to a modal group index change of 1.5%. This is sufficient to demonstrate the full tuning range of the SGDBR device.

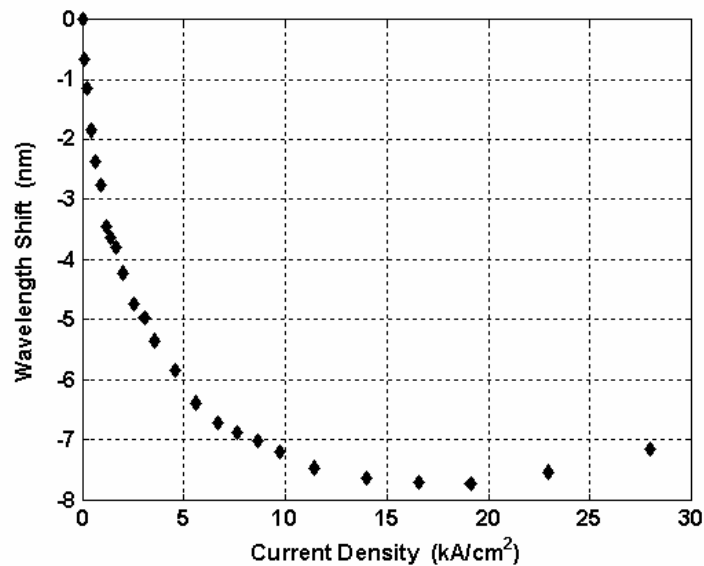


Figure 16. Wavelength shift as a function of current density

3.8. Buried hetero-structure SGDBR laser

The SGDBRs, incorporating a centered quantum well active region, and fabricated using QWI to render three band-edges, exhibit low threshold current and high output power. Operating in continuous-wave mode, the power out versus applied bias was measured for a 7 quantum well SGDBR. As shown in Fig. 17, the SGDBR produces more than 20 mW of output power with a 100 mA bias on the gain section. The threshold current was measured to be 10.4 mA, with a

slope efficiency of 25%. This low threshold current is made possible by the high modal gain achievable using the centered quantum well design.

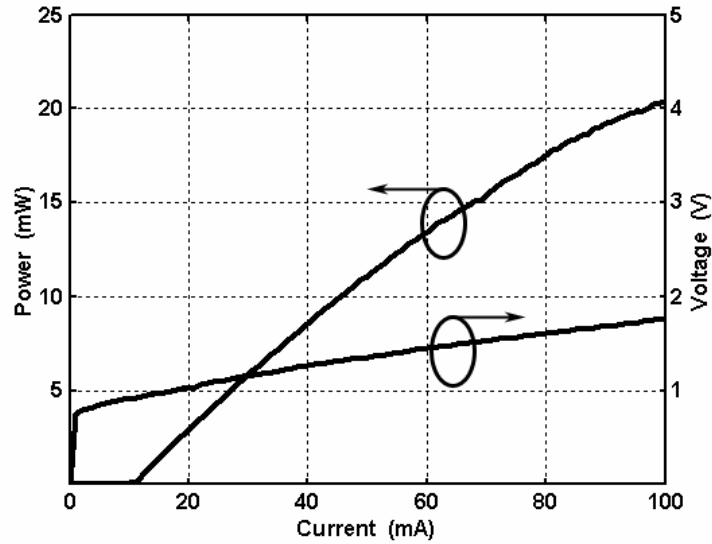


Figure 17. untuned CW SGDBR LIV Characteristics

3.9. EAM Extinction and Bandwidth

In this section we report the data obtained from the ten quantum well active region design. The EAM bandgap was placed at 1495 nm using the previously described process, and is shown in the photoluminescence curve in Fig. 45. The length of the EAM is 175 microns.

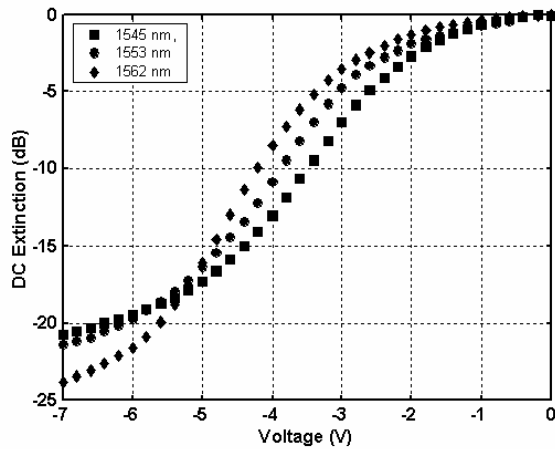


Figure 18. DC extinction for 10QW design

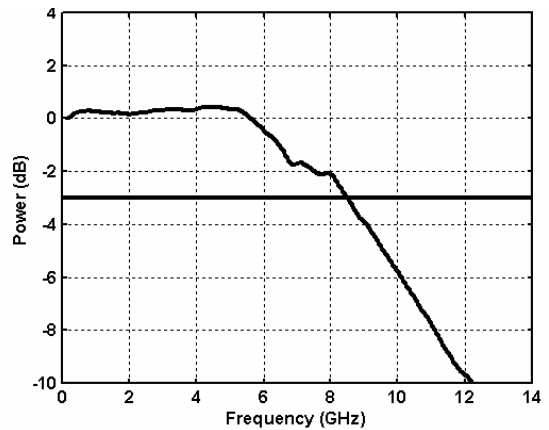


Figure 19. QWI EAM 3dB Bandwidth

The DC extinction was measured for three wavelengths over the tuning band. Approximately 20 dB of extinction was observed at -6 volts. This data is illustrated in Fig. 18. The RF bandwidth was characterized using a light-wave impedance analyzer. As shown in Fig. 19, the 3dB bandwidth was measured to be 8.5 GHz at 1553 nm and a DC bias of -4 volts.

3.10. Conclusions

We have demonstrated a buried hetero-structure based SGDBR with integrated EAM using quantum well intermixing. This is a promising technology to tailor the absorption properties in various sections in photonic integrated circuits. In the case of the SGDBR-EAM device, we have demonstrated 3 different band-edges with the potential for many more in devices that may require them.

4. Other Integration Possibilities

4.1. Wavelength Converters

As dynamically configured networks emerge, devices that can convert one WDM wavelength to another become in demand [11-14]. One approach of fabricating a tunable wavelength converter involves the integration of a SGDBR and detector along with biasing circuitry (OEIC PD-SGDBR). Alternatively, by integrating a SGDBR with a Mach-Zehnder with SOAs in each branch, purely optical wavelength conversion can be performed. This is achieved by the use of cross-phase modulation where the change in intensity of light from the input effectively changes the index in one branch of the all-active Mach-Zehnder interferometer which results in a change in the output intensity. In each case, wavelength conversion can be performed using only DC biases so off-chip RF packaging is not necessary.

4.2. Biosensors

Heterodyned signals from two lasers provide a very sensitive detection scheme. One approach of realizing a biosensor involves the integration of two SGDBRs with an MMI combiner and detector [22]. One laser is designed in which part of the dielectric is removed, allowing a perturbation of the modal index in this laser when a liquid or biomaterial is applied to the surface. By measuring the beat frequency between the two lasers, one can detect minute changes in index. By tuning the lasers over a wide range, spectral signatures of different materials can be assessed. No coupling of light on and off chip is necessary for operation simplifying the packaging greatly.

5. REFERENCES

- [1] Coldren, L. A., "Monolithic Tunable Diode Lasers", *IEEE Journal Special Topics Quantum Electronics.*, 6, No. 6, Nov. 2000.
- [2] Akage, Y.; Kawano, K.; Oku, S.; Iga, R.; Okamoto, H.; Miyamoto, Y.; Takeuchi, H. "Wide bandwidth of over 50 GHz travelling-wave electrode electroabsorption modulator integrated DFB lasers," *Electronics Letters*, 37, IEE., 299-300. (2001)
- [3] Xun, Li, W.-P Huang, D. M. Adams, C. Rolland, T. Makino, "Modelling and Design of a DFB Laser Integrated with a Mach Zehnder Modulator," *IEEE. J. Quantum Electronics*, 34. (1998).
- [4] Mason, B.; J.S. Barton, G. A. Fish, L.A. Coldren, S.P. Denbaars, "Design of sampled grating DBR lasers with integrated semiconductor optical amplifiers," *IEEE Photonics Technology Letters*, 12, IEEE, 762-4. (2000)
- [5] Mason, B., G. A. Fish, S.P. DenBaars, and L.A. Coldren, "Widely Tunable Sampled Grating DBR Laser with Integrated Electroabsorption Modulator," *IEEE. Photon. Tech. Letts*, 11, 638-640, (1999).
- [6] Barton, J. S., E.J. Skogen, M.L. Mašanović, Steven P. DenBaars, Larry A. Coldren, "Monolithic integration of Mach-Zehnder modulators with Sampled Grating Distributed Bragg Reflector lasers", *Proc. Integrated Photonics Research 2002 Conference*, Vancouver, Canada
- [7] Barton, J. S., Erik J. Skogen, Milan L. Mašanović, Steven P. DenBaars, Larry A. Coldren, "Tailorable chirp using Integrated Mach-Zehnder modulators with tunable Sampled Grating Distributed Bragg Reflector lasers", *Proc. International Semiconductor Laser Conference Garmisch-Partenkirchen*, 2002.
- [8] Fish, G.A. (Edited by: Sawchuk, A.A.) "Monolithic widely-tunable DBR lasers," OFC 2001. *Optical Fiber Communication Conference and Exhibit. Technical Digest Postconference Edition* (IEEE Cat. 01CH37171), 2, OFC (2001).
- [9] V. Jayaraman, Z. Chuang, and L. Coldren, "Theory, Design, and Performance of Extended Tuning Range Semiconductor Lasers with Sampled Gratings," *IEEE J. Quantum Electron.*, vol. 29, pp. 1824-1834, 1993.
- [10] Devaux, F. Y. Sorel, J.F. Kerdiles, "Simple Measurements of Fiber Dispersion and of Chirp Parameter of Intensity Modulated Light Emitter" *J. Lightwave Tech.* 11., No. 12, Dec. 1993.
- [11] X. Pan, J.M. Wiesenfeld, J.S. Perino, T.L. Koch, G. Raybon, U. Koren, M. Chien, M. Young, B.I. Miller, C.A. Burrus, "Dynamic Operation of a Three-Port, Integrated Mach-Zehnder Wavelength Converter", - *IEEE Photonics Technology Letters*, 7, IEEE, 995-97. (1995)
- [12] W. Idler, K. Daub, G. Laube, M. Schilling, P. Wiedemann, K. Dutting, M. Klenk, E. Lach, K. Wunstel, "10 Gb/s Wavelength Conversion with Integrated Multiquantum-Well 3-Port Mach-Zehnder Interferometer" - *IEEE Photonics Technology Letters*, 8, IEEE, 1163-65. (1996)
- [13] C. Janz, F. Poingt, F. Pommereau, W. Grieshaber, F. Gaborit, D. Leclerc, I. Guillemot, M. Renaud, "New All Active Dual Order Mode (DOMO) Mach-Zehnder Wavelength Converter For 10 Gbit/s Operation", *Proc. ECOC 99*, Nice, France

- [14] L.H. Spiekman, U. Koren, M.D. Chien, B.I. Miller, J.M. Wiesenfeld, J.S. Perino, "All-Optical Mach-Zehnder Wavelength Converter with Monolithically Integrated DFB Probe Source", *IEEE Photonics Technology Letters*, **9**, IEEE, 1349-51. (1997)
- [15] E. Skogen, J. Barton, S. DenBaars, and L. Coldren, "A Quantum-Well-Intermixing Process for Wavelength-Agile Photonic Integrated Circuits," *IEEE J. Sel. Topics in Quantum Electron.*, **8**, pp. 863-869, 2002.
- [16] N. Holonyak, Jr., "Impurity-Induced Layer Disordering of Quantum-Well Heterostructures: Discovery and Prospects," *IEEE J. Sel. Topics in Quantum Electron.*, **4**, pp. 584-594, 1998.
- [17] S. K. Si, D. H. Yeo, K. H. Yoon, and S. J. Kim, "Area Selectivity of InGaAsP-InP Multi-quantum-Well Intermixing by Impurity-Free Vacancy Diffusion," *IEEE J. Sel. Topics in Quantum Electron.*, **4**, pp. 619-623, 1998.
- [18] A. McKee, C. McLean, G. Lullo, A. Bryce, R. De La Rue, J. Marsh, and C. Button, "Monolithic integration in InGaAs-InGaAsP multiple-quantum-well structures using laser intermixing," *IEEE J. Quantum Electron.*, **33**, pp.45-55, 1997.
- [19] S. Charbonneau, E. Kotels, P. Poole, J. He, G. Aers, J. Haysom, M. Buchanan, Y. Feng, A. Delage, F. Yang, M. Davies, R. Goldberg, P. Piva, and I. Mitchell, "Photonic Integrated Circuits Fabricated Using Ion Implantation," *IEEE J. Sel. Topics in Quantum Electron.*, **4**, pp. 772-793, 1998.
- [20] M. Paquette, J. Beauvais, J. Beerens, P. Poole, S. Charbonneau, C. Miner, and C. Blaauw, "Blueshifting of InGaAsP/InP laser diodes by low-energy ion implantation," *Appl. Phys. Lett.*, **71**, pp. 3749-3751, 1997.
- [21] M. Amann, and W. Thulke, "Current Confinement and Leakage Currents in Planar Buried-Ridge-Structure Laser Diodes on n-Substrate," *IEEE J. Quantum Electron.*, **25**, pp. 1595-1602, 1989.
- [22] D. A. Cohen, E. J. Skogen, H. Marchand, L.A. Coldren, "Monolithic Chemical Sensor Using Tandem Heterodyned Sampled Grating DBR Lasers." *Elect. Letts*, **37**, (22), 1358-60, (Oct 25, 2001).